Replication of surface micro-features using variothermal injection moulding: application to micro-fluidics

Journal:	*Polymer Engineering & Science*
Manuscript ID	PES-17-0161.R1
Wiley - Manuscript type:	Research Article
Date Submitted by the Author:	07-Nov-2017
Complete List of Authors:	Wlodarski, P G; Swansea University, ASTUTE2020, College of Engineering, Bay Campus Pittman, John; Swansea , ASTUTE20202, College of Engineering
Keywords:	injection molding, glass transition, surfaces

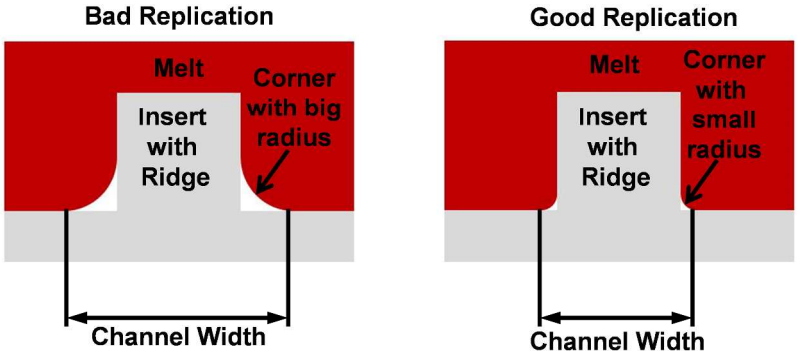

Figure 1: Schematic of a cross section through a molded channel and the insert ridge showing rounded upper channel corners on the moldings corresponding to poor and good replication.

793x595mm (96 x 96 DPI)

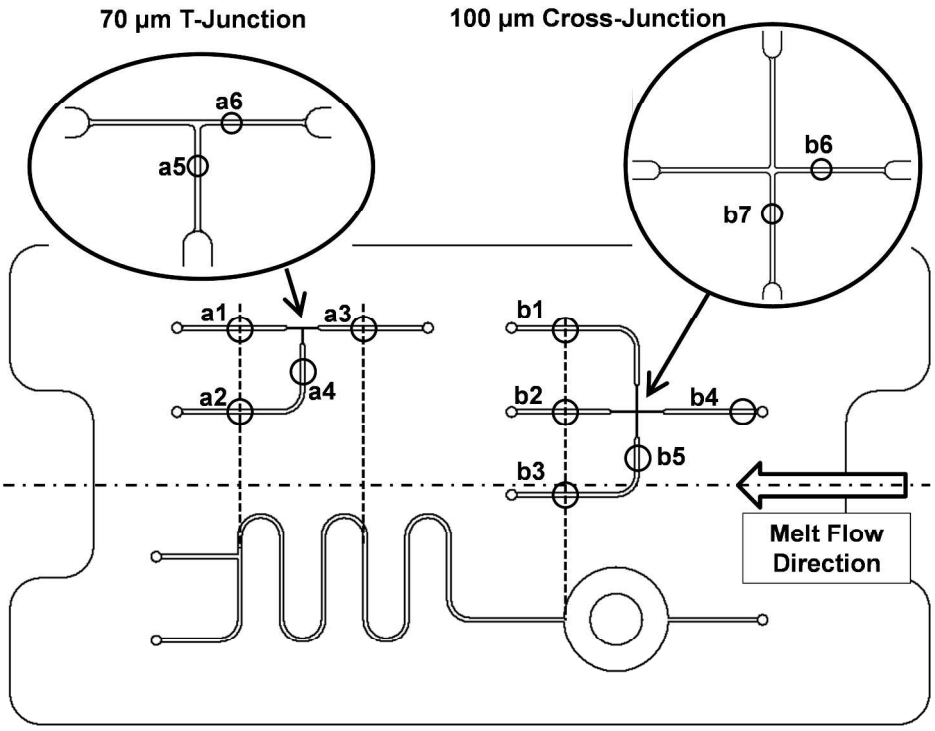

Figure 2: Insert for micro-fluidic feature molding, with examination positions of the injection molded chip. Overall dimensions of the insert: 88 x 46 mm.

793x595mm (96 x 96 DPI)

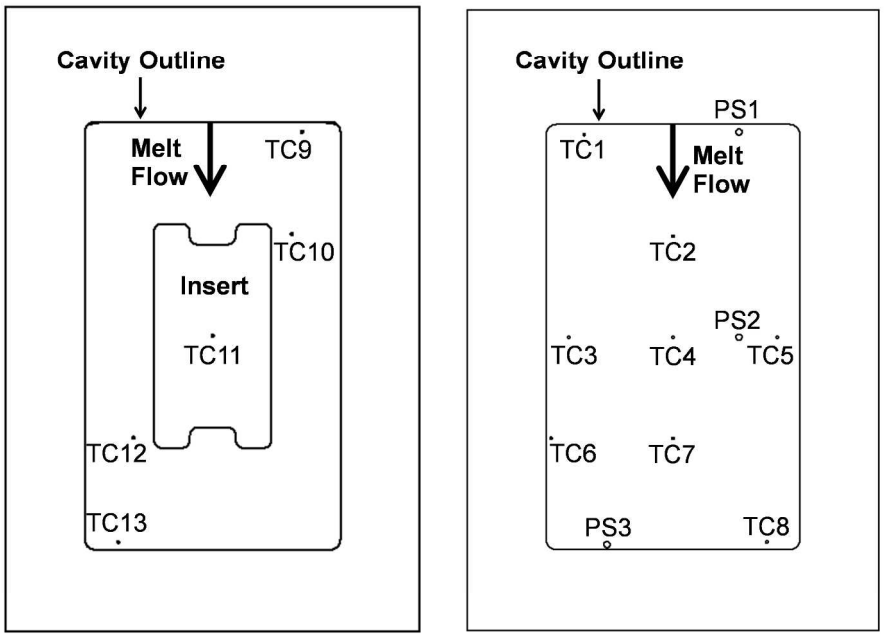

Figure 3: Thermocouple (TC) and pressure sensor (PS) locations in moving (left) and fixed (right) tool halves.

793x595mm (96 x 96 DPI)

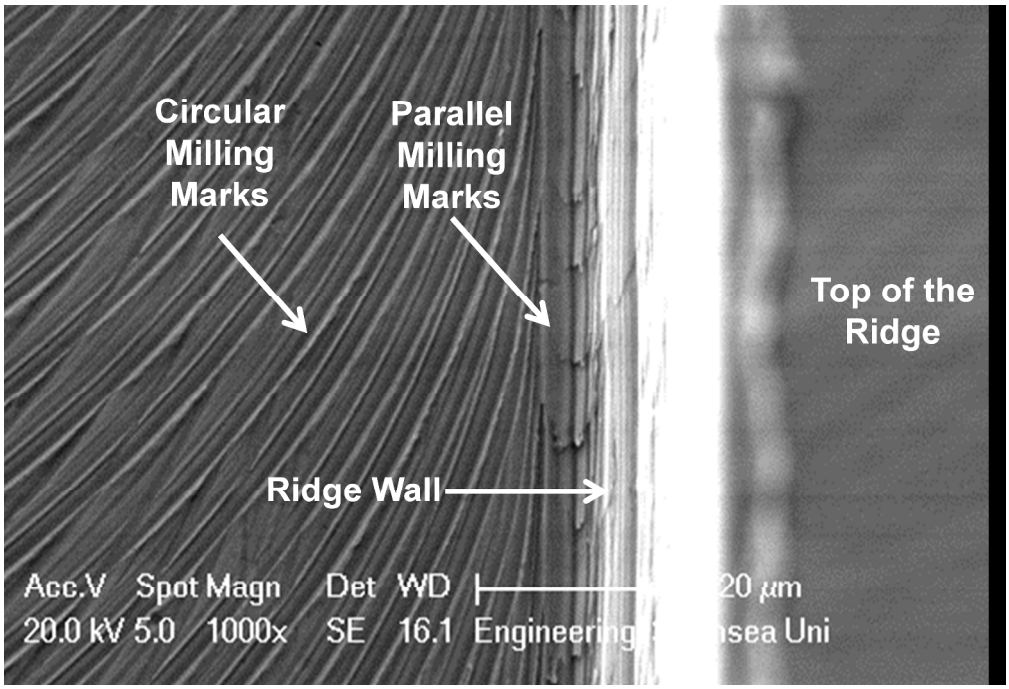

Figure 4: SEM image of the bottom corner of a 400 μm ridge on the mold insert.

1146x778mm (96 x 96 DPI)

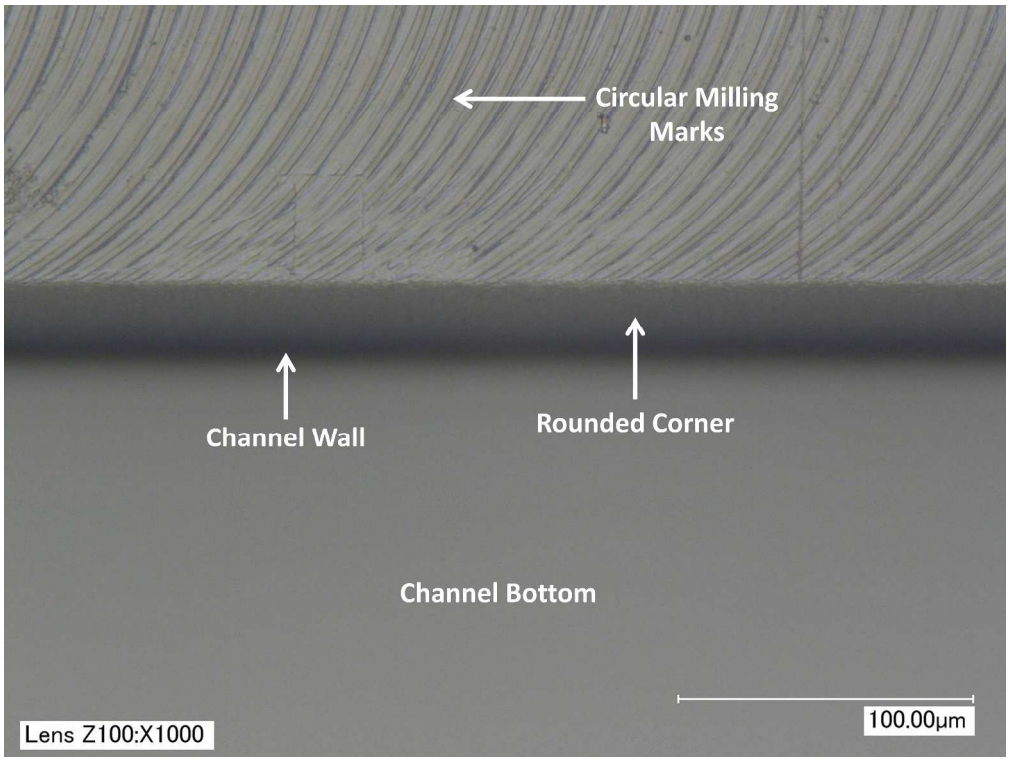

Figure 5: Digital microscope image of a molding produced at processing condition A at Position a2. Close up of one channel side showing a rounded upper corner and failure to transcribe milling marks adjacent to the insert ridge.

1510x1132mm (96 x 96 DPI)

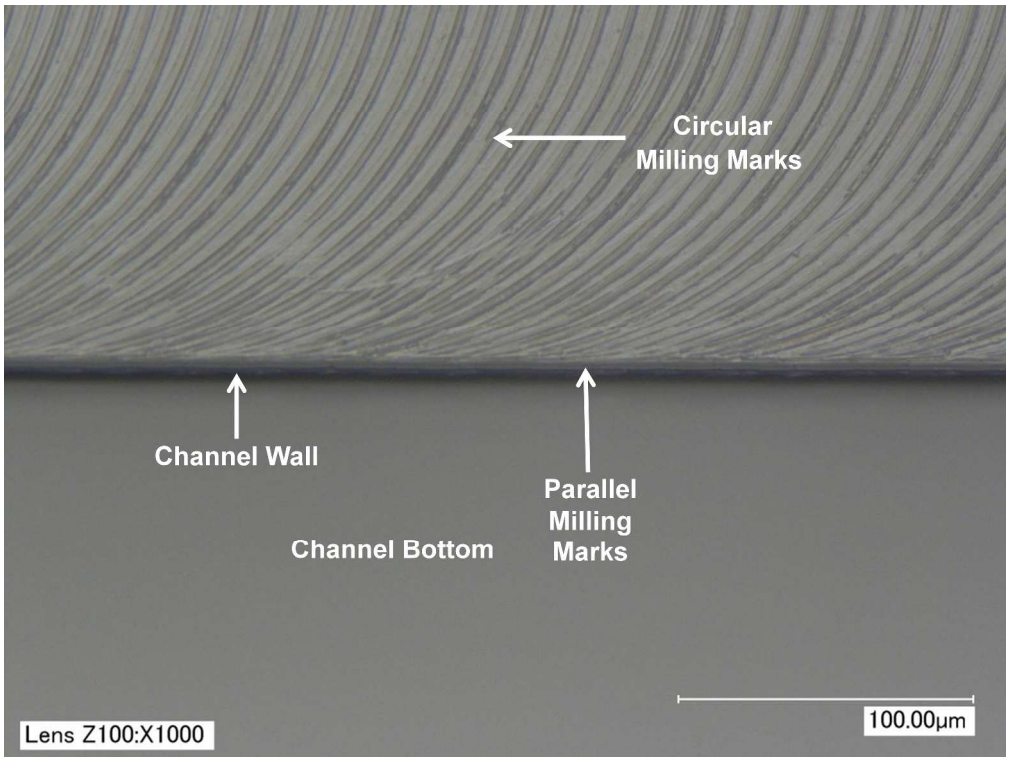

Figure 6: Digital microscope image of a molding produced at processing condition C at position a2. Close up of one channel side showing a very narrow rounded corner and more complete transcription of milling marks.

1508x1131mm (96 x 96 DPI)

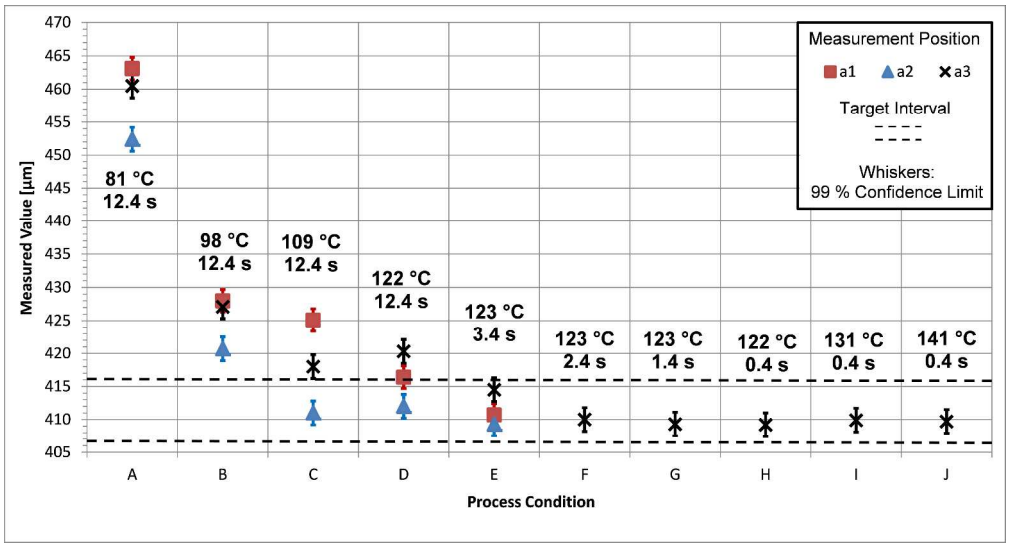

Figure 7: Measurements of 400 µm channel top width at indicated positions for different processing conditions.

1796x963mm (96 x 96 DPI)

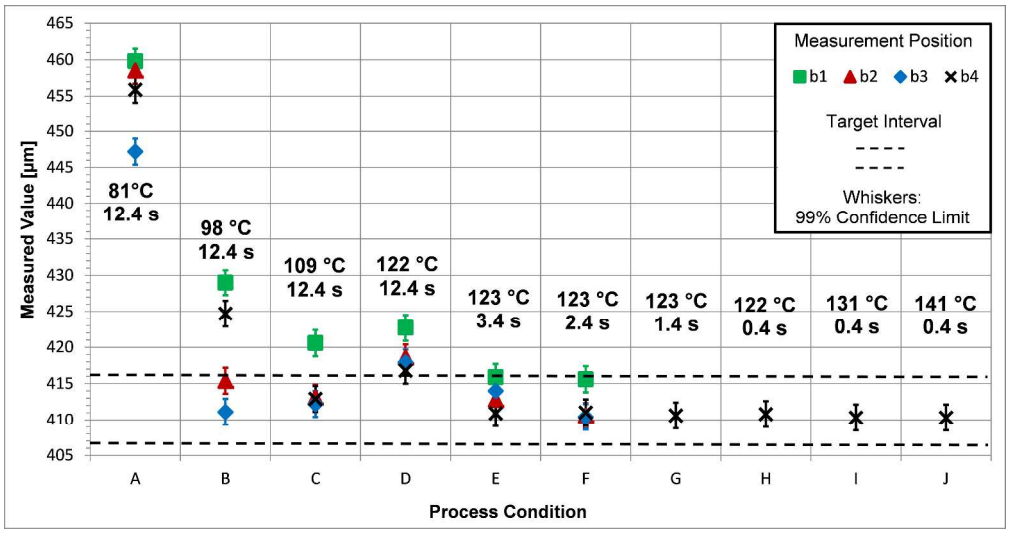

Figure 8: Measurements of 400 µm channel top width at indicated positions for different processing conditions.

1725x901mm (96 x 96 DPI)

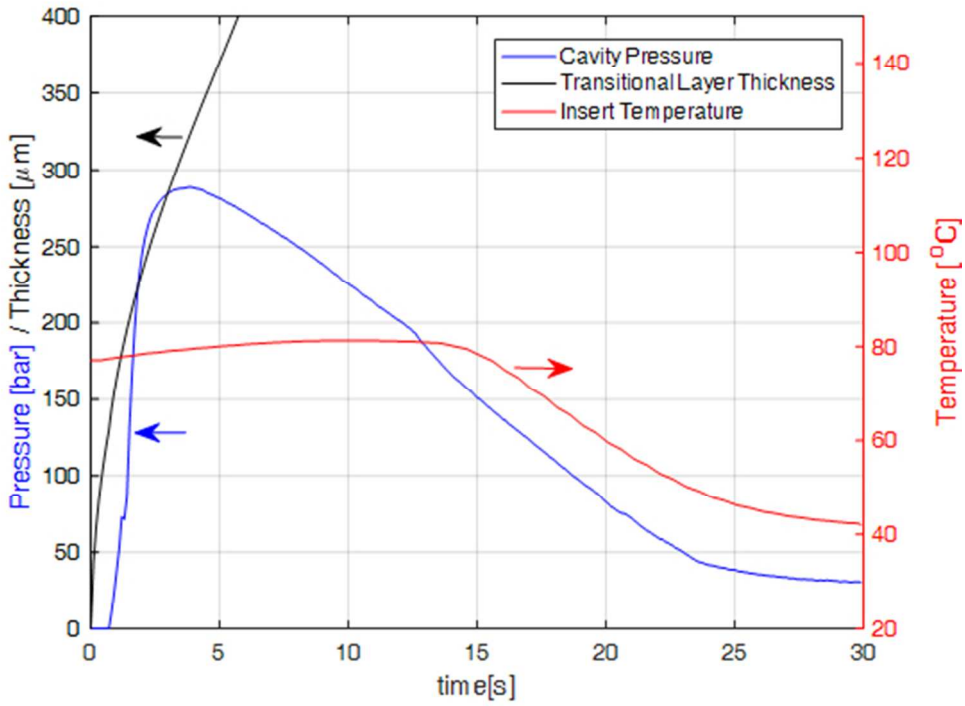

Figure 9: Cavity pressure, transitional layer development, and insert surface temperature for process condition A.

148x111mm (96 x 96 DPI)

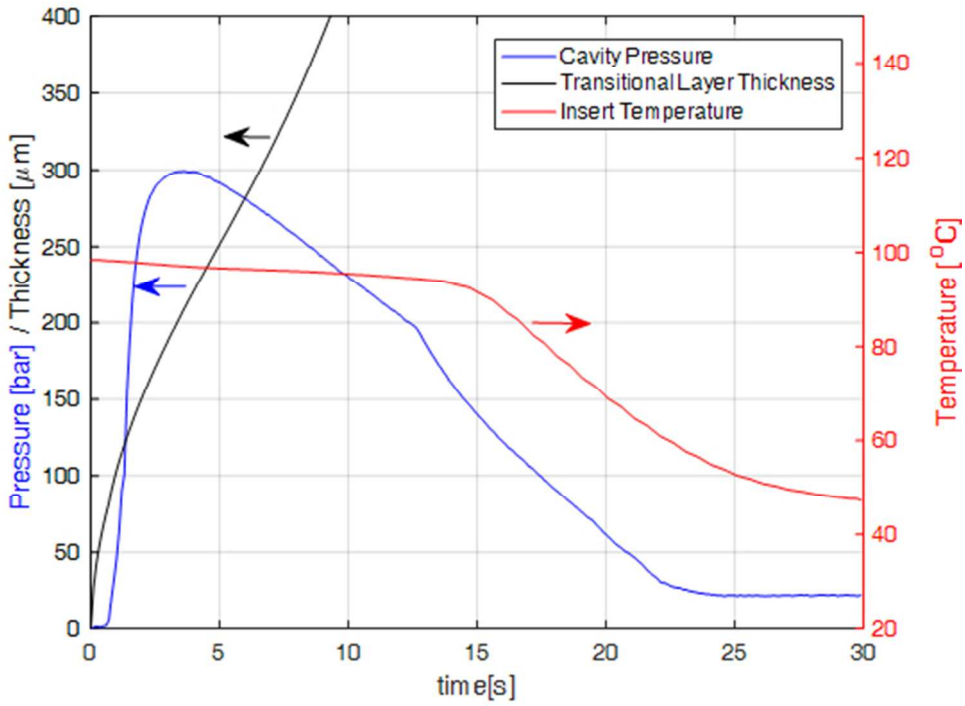

Figure 10: Cavity pressure, transitional layer development, and insert surface temperature for process condition B.

148x111mm (96 x 96 DPI)

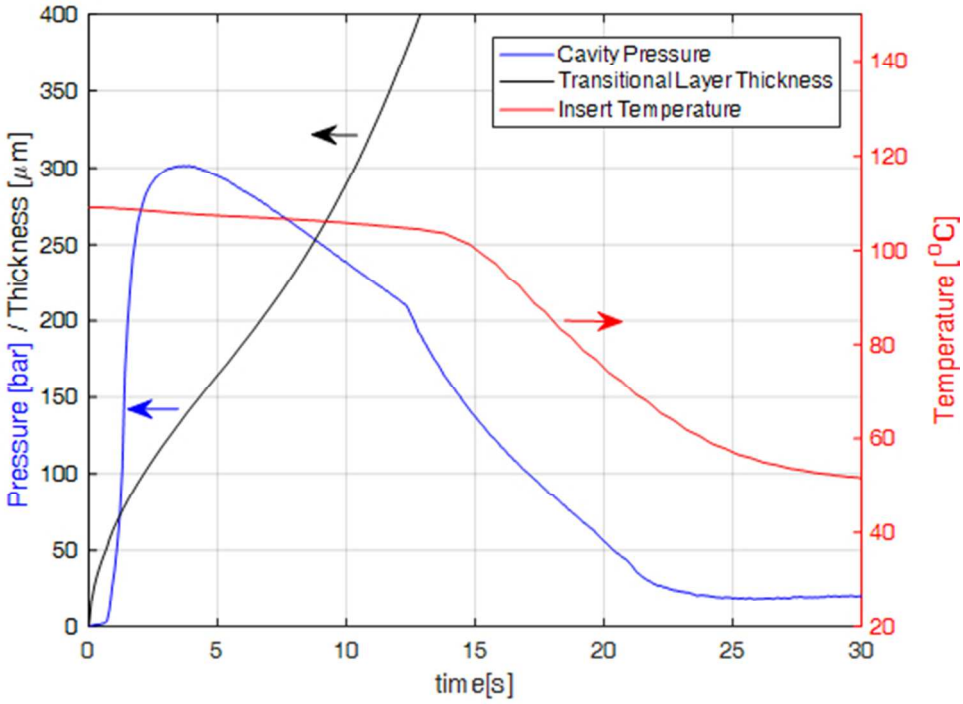

Figure 11: Cavity pressure, transitional layer development, and insert surface temperature for process condition C.

148x111mm (96 x 96 DPI)

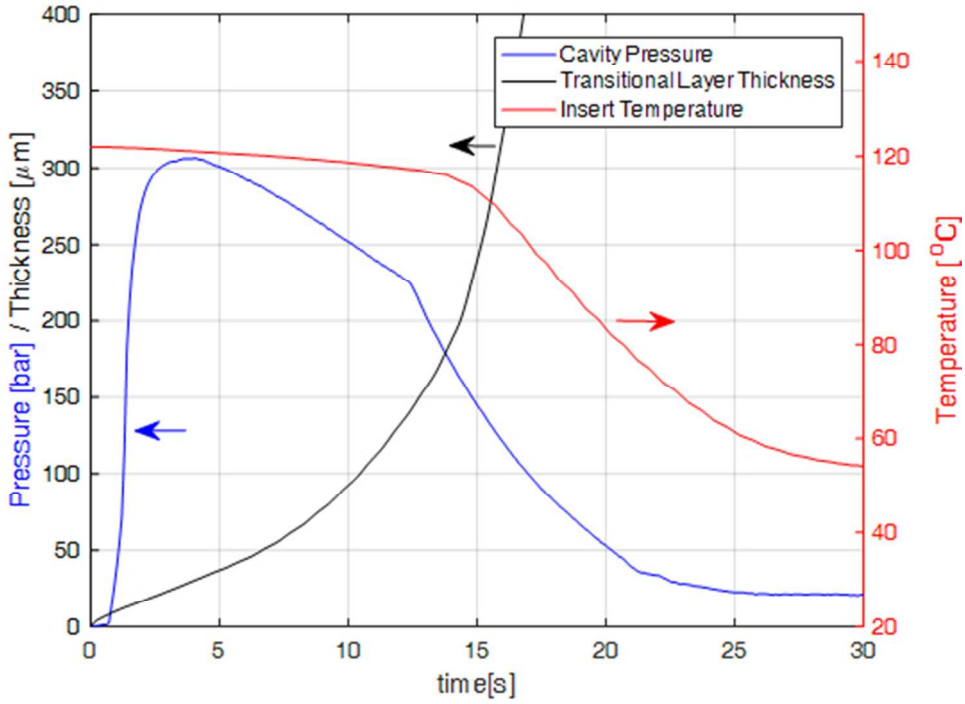

Figure 12: Cavity pressure, transitional layer development, and insert surface temperature for process condition D.

148x111mm (96 x 96 DPI)

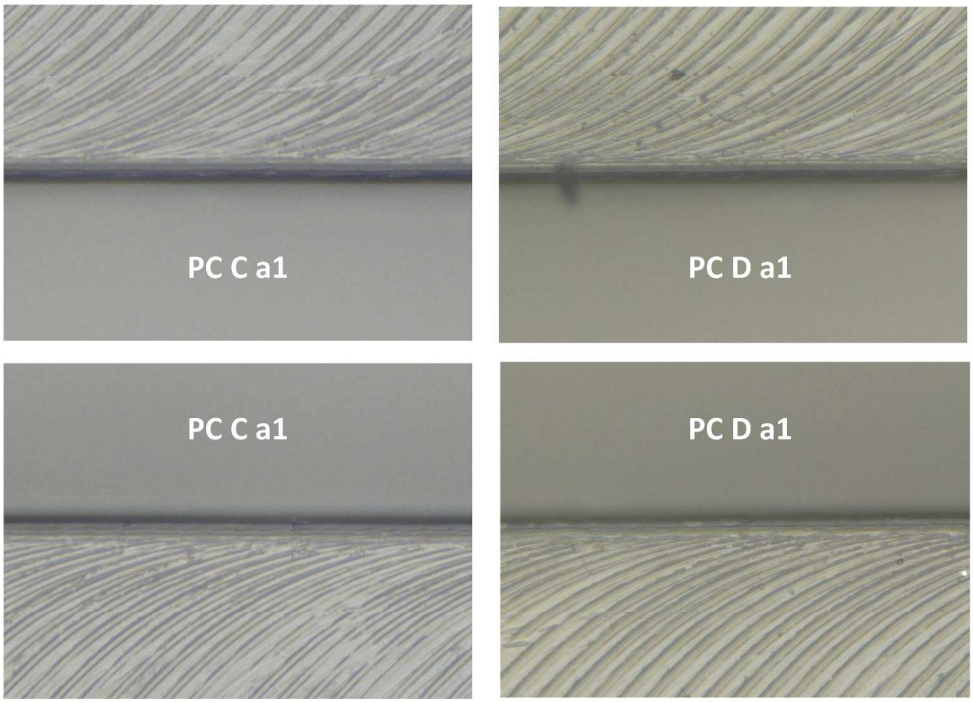

Figure 13: Comparison of replication between process conditions C and D, showing how milling marks are equally well replicated.

793x595mm (96 x 96 DPI)

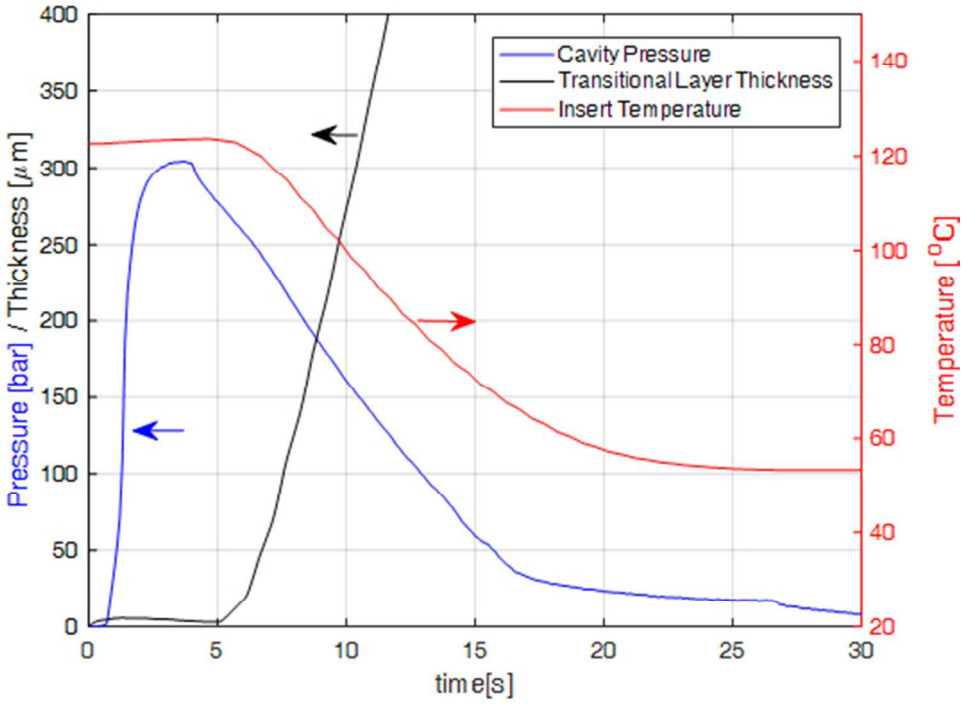

Figure 14: Cavity pressure transitional layer development, and insert surface temperature for process condition E.

148x111mm (96 x 96 DPI)

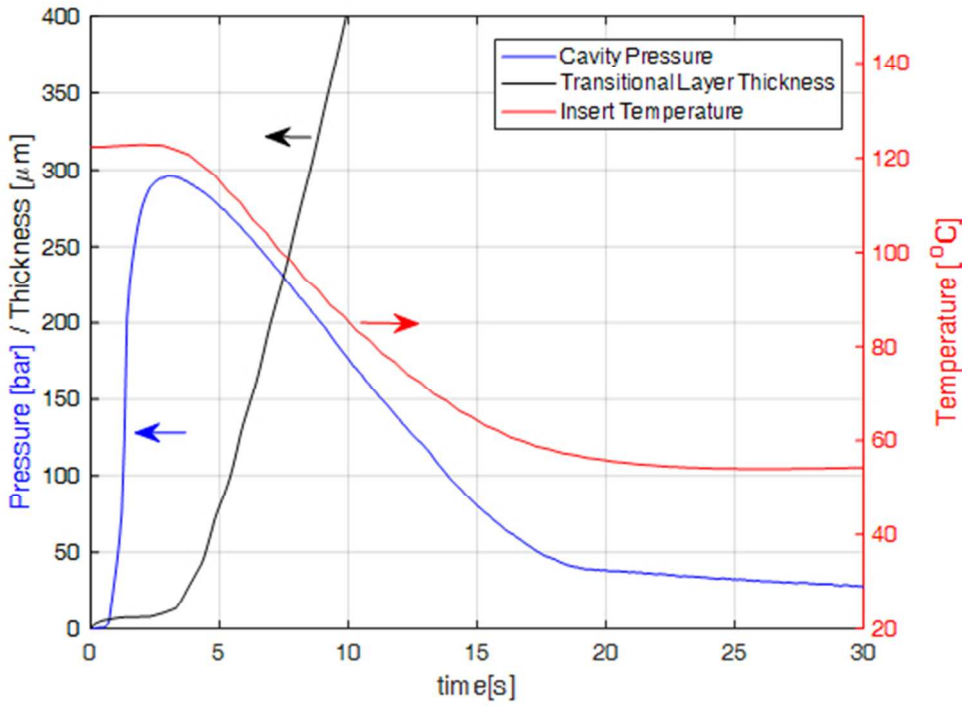

Figure 15: Cavity pressure, transitional layer development, and insert surface temperature for process condition G.

148x111mm (96 x 96 DPI)

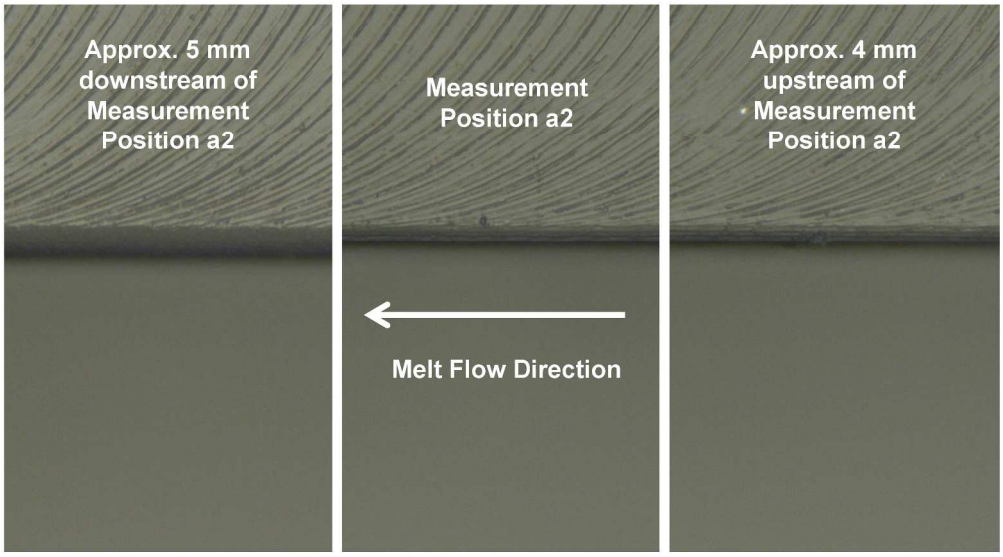

Figure 16: Transition in replication quality along the channel including measurement position a2 for process condition G.

793x595mm (96 x 96 DPI)

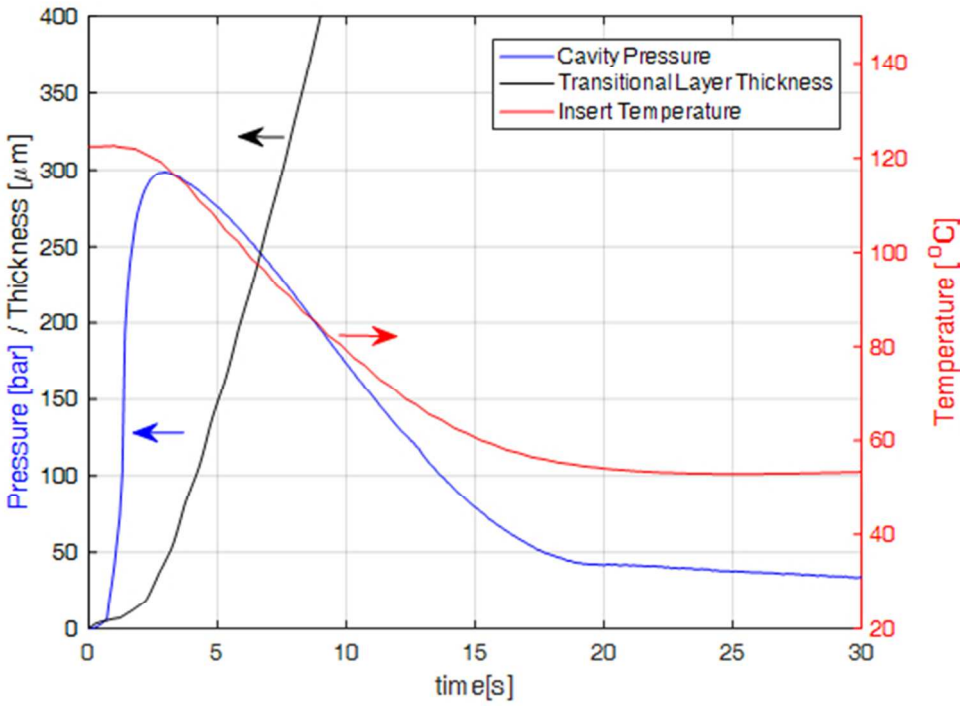

Figure 17: Cavity pressure, transitional layer development, and insert surface temperature for process condition H.

148x111mm (96 x 96 DPI)

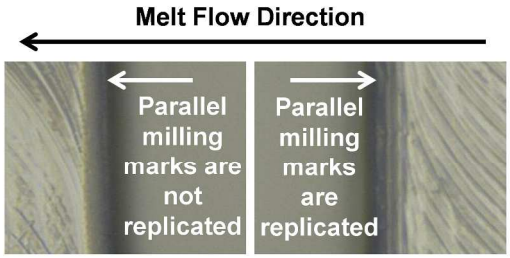

Figure 18: Digital microscope image for process condition G at position a4. On the downstream side of the melt flow direction the parallel milling marks are not replicated.

793x595mm (96 x 96 DPI)

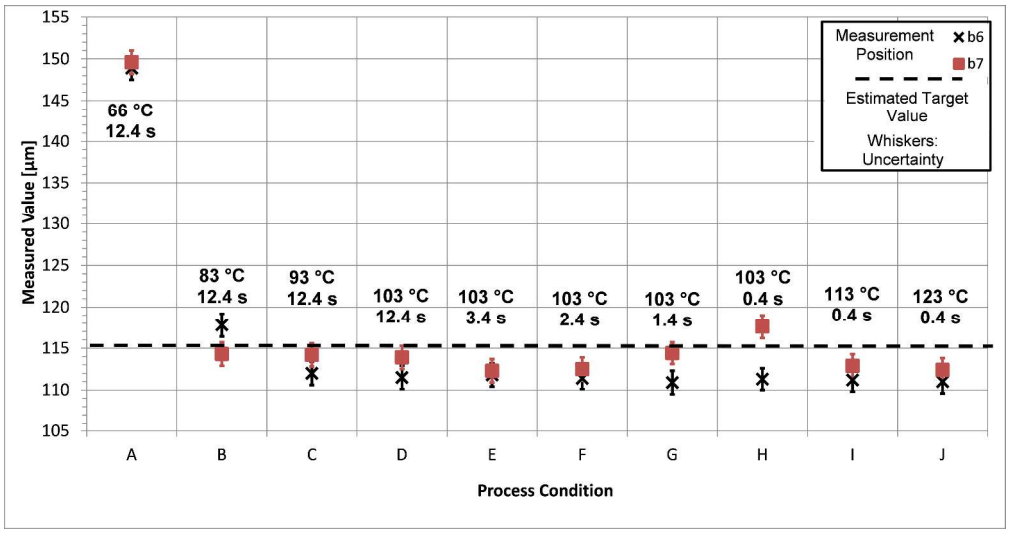

Figure 19: Measurements of 100 µm channel top width at indicated positions for different processing conditions. Whiskers indicate 99% confidence limits.

1921x1005mm (96 x 96 DPI)

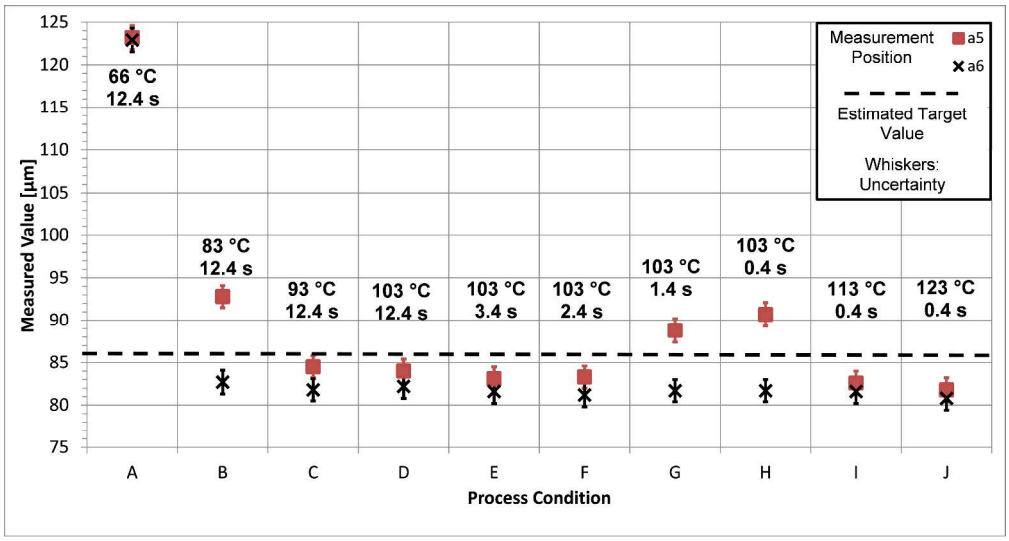

Figure 20: Measurements of 70 µm channel top width at indicated positions for different processing conditions. Whiskers indicate 99% confidence limits.

1819x963mm (96 x 96 DPI)

Table 1: Thermal Properties of Steel and PMMA

	Steel	PMMA
Thermal Conductivity [W/m K]	24.9	0.1833
Density [kg/m^3]	7740	1125
Specific Heat [J/kg K]	460	1874
Calculated Effusivity [W $s^{1/2}/m^2$ K]	9415.6	621.6

Process Condition	Mould Insert Temperature TC 11 [°C]	Max Cavity Pressure Sensor 2 [bar]	Active Cooling [s] after Injection Start
A	81	288	12.3
B	98	299	12.3
C	109	301	12.4
D	122	306	12.4
E	123	304	3.4
F	123	296	2.4
G	123	296	1.4
H	122	294	0.4
I	131	302	0.4
J	141	303	0.4

Table 2: Processing Conditions.

Replication of surface micro-features using variothermal injection molding: application to micro-fluidics

P. G. Wlodarski, J. F. T. Pittman*

p.wlodarski@swansea.ac.uk, j.f.t.pittman@swansea.ac.uk, 0044 (0)1792 295732
ASTUTE2020, College of Engineering, Swansea University,
A006 Engineering Central, Bay Campus, Swansea University, SA1 8EN, UK.

Abstract

We study injection molding of meso-scale items with µm-scale surface features, namely micro-fluidic channels, relating replication quality to process conditions. Using variothermal molding the variables are the pre-heat temperature of the cavity insert surface before melt injection and the mold cooling start time. Surface temperatures and in-cavity melt pressures are continuously measured. Rounded upper corners of the micro-channels are used as an index of replication quality. For polymethylmethacrylate the thickness of a layer with solid-like properties (below 124°C) is calculated and used with pressures to interpret results. It is shown how improved replication correlates with low layer thickness at the end of the compression phase when pressures are at a maximum, and the necessity of properly timed cooling to lock in replication before melt pressures fall. Results show how the inter-relationship of layer thickness and melt pressure is controlled by pre-heat temperature and cooling switch-on time. Delayed cooling can result in poorer replication, due to a retraction effect of the plastic. Too early cooling also reduces replication of parallel-to-flow features downstream of transverse features, and of the replication of transverse features on their downstream side. Good replication of 100 and 70µm channels requires lower pre-heat than 400µm ones.

Key words: Processing technologies, injection molding, micro-feature replication, micro-fluidics, variothermal molding.

1. Introduction

This work studies the use of thermoplastics injection molding to produce parts carrying functional surface features with dimensions in the micron size range. As distinct from the production of micro-parts using a micro-injection molding machine, we are concerned here with meso-scale items, with overall dimensions usually of a few centimeters, produced using a conventional molding machine. Molding such parts makes possible the integration of micro-features with meso-scale details providing connections and interaction with the everyday macro-world. Injection molding is particularly suitable for low cost, large volume production. Furthermore, parts with complex geometries and multiple features can be produced requiring little or no finishing.

Application areas include but are not limited to micro-optics (light guides, diffractive elements, micro-lens arrays ….), bio-mimetic surfaces (antireflective, dry adhesion, drag reduction, super-hydrophobicity ….) and micro-fluidics. The latter is the focus of the present work.

Reference (*1*) provides a recent review of the present and future role of micro-fluidics in biomedical research and points out that publication rate is high and dominated by articles in engineering journals. This reflects the difficulties of translating engineering research on production of micro-total-analysis or lab-on-a-chip devices to applications in biology and biomedical research and wider applications in the field. An important factor is material selection, both with regard to material properties and potential for manufacturing methods. Since the 1980s the field has been dominated by polydimethylsiloxane (PDMS), which provides simple, cheap set-up in the research environment. However, some physical properties are problematic, and manufacture is not easily scaled to large volume production. Injection molding of thermoplastics, such as polymethylmethacrylate (PMMA),

polycarbonate (PC), cyclic olefin copolymer (COC) or polystyrene (PS), as well as thermoplastic elastomers, has the potential to overcome these limitations. These materials provide a wide choice of properties selectable for specific applications, such as optical clarity, biocompatibility, and hydrophilicity or hydrophobicity. Crucially, they are suited to rapid, large volume production methods. Among these, injection molding provides shorter cycle times than hot embossing, and is capable of producing devices with integrated three-dimensional meso-scale features which essentially two-dimensional processes such as embossing and rolling cannot do. Potential applications for low cost, mass produced micro-fluidics are widespread. Single use, disposable, point-of-care diagnostics can be transformative for the delivery of healthcare. Ultra-low fluid volumes, introduced by capillary action, simplify testing and can reduce analysis times substantially. These advantages and other unique features of micro-fluidic processing are also relevant in a research and development setting, allowing studies that would not be possible using conventional methods. In order to realize this potential, accurate replication of the micro-features by the injection molding process is essential. This requires a clear understanding of the relationship between processing parameters and outcomes. Failure to achieve the correct dimensions or geometry can adversely affect the functioning of micro-fluidic devices. Fluid volumes may not conform to design, and details of required flow patterns may be perturbed. Most micro-fluidic devices require closed channels, necessitating a post-processing step to seal the channels by applying a cover plate or film, attached using welding, adhesives or other bonding method. A common defect in molded channels is the occurrence of rounded upper corners instead of the sharp corners defined by the master (mold insert), see Figure 1. As well as affecting fluid volumes and hold up times, these can make the sealing process more difficult.

The occurrence of rounded upper channel corners is the focus of the present work and is used as an index of replication quality.

Fabrication technologies for polymeric micro-fluidic devices are reviewed by (*2*), comparing injection molding with other replication processes. A more general review of the replication of micro- and nano-geometries in a range of materials is provided by (*3*), which also includes master making. The master is the negative of the required molded features, and is usually in the form of an insert in the mold tool. To produce micro-fluidic channels it will have raised ridges. An extensive literature exists on micro-manufacturing in general (*4, 5*) and for the production of mold insert masters for micro-fluidics (*5, 6*). The reader is referred to these and similar publications for further details of these topics.

De-molding of the plastic part can in some cases reduce replication quality by damaging the micro-features. This topic is not included in the present work. The present objective is to better understand how the injection molding process conditions during filling, compression and holding influence replication accuracy in the molding of micro-fluidic channels, together with the influence of the micro-feature location, size and orientation. Though the present work is focused on micro-fluidic channels, the insights provided will be relevant to replication of other micro-features by injection molding.

The layout of the paper is as follows. The main conclusions of previous work examining the replication of micro- and nano-features by injection molding are summarized, followed by a brief review of the molding of recessed features such as micro-fluidic channels. The test problem in the present work is then introduced, followed by a description of the experimental mold and the master insert for molding micro-fluidic circuits. The procedure for the assessment of replication quality is explained; this measures the increase in the upper width of the molded channels due to the formation of rounded corners, see Figure 1. The molding

process and equipment are next described. These implement variothermal injection molding, where the mold is pre-heated before polymer injection and then rapidly cooled. An important feature is the inclusion of comprehensive temperature and pressure measurement in the mold cavity, which provides simultaneous melt pressures and mold surface temperatures at the location of the master insert and elsewhere, throughout the molding cycle. A program of molding trials is described in which the mold insert pre-heat temperature and the cooling switch-on time are varied. To assist with interpretation of the trial results, cooling of the plastic is simulated numerically, using the measured transient insert surface temperatures as boundary condition. Changes in the mechanical properties of the plastic around the glass transition temperature are reviewed, and the thickness of a cooled layer having properties that would hinder replication is calculated as cooling proceeds. Results for replication quality are then introduced and interpreted in terms of cooled layer thicknesses and the prevailing melt pressures. Additionally, effects of micro-feature location, orientation and size are identified.

2. Replication of Micro-features in Injection Molding

2.1. Overview

A qualitative description of the replication process is provided by (*7*). Initially the mold cavity fills and the melt flow passes over the micro-features. With a cold cavity surface, a highly viscous layer immediately starts to form and grows into a frozen layer. Melt pressure during filling is relatively low, often providing little driving force for melt to flow into or around the micro-features. At the end of filling the melt pressure rises rapidly in the compression phase and is maintained during holding, reducing as freezing progresses. Under these higher pressures plastic may be forced fully into contact with the micro-features, undergoing deformation resisted by viscous, plastic and elastic forces (*8*). Completion of

freezing locks in the deformation, with holding pressure applying packing to compensate for shrinkage.

The literature in this area is extensive and here we highlight the key conclusions. Many studies have taken a design-of-experiments approach to investigate the relative importance of the various injection molding process parameters, but, since each is usually varied at only two or three levels, these provide limited insight into the detailed mechanisms of action and interaction (*9-16*). In the following paragraphs the important process parameters are identified, with an outline of how and why they influence replication, illustrated by selected citations. This is followed by comments on works specifically concerned with molding micro-fluidic channels.

2.2. Melt and mold cavity surface temperature

Since the formation of a viscous or solidified layer hinders replication, it is widely recognized that replication is improved by raising melt injection temperature (*7, 11, 17-23*) or cavity (insert) surface temperature (*7, 11, 15, 16, 18, 20, 22-29*). Raising these temperatures while keeping other parameters fixed will, however, reduce filling pressure. Where replication occurs mainly during filling, this can have an adverse effect (*13*).

The initial temperature at the polymer-metal interface (T_{IF}) during filling, as the fountain flow lays down melt (at temperature T_M) on the cavity surface (at T_S), is often estimated using the analytic solution for heat conduction in two semi-infinite slabs brought suddenly into contact (*30*), Equation (1).

$$T_{IF} = \frac{1}{e_M + e_S}\left(e_M T_M + e_S T_S\right) \quad \textbf{(1)}$$

where e_M and e_S are the effusivities of the melt and mold material, being the square root of the product of thermal conductivity, density and specific heat. Table 1 provides values for PMMA and tool steel. The effusivity of PMMA, as indeed of typical plastics, is an order of magnitude smaller than that of tool steel, showing that the initial interfacial temperature will be more strongly influenced by the cavity surface temperature. This is why it is usually found that cavity surface temperature has a stronger influence than the melt temperature, and why pre-heating the cavity surface to around the glass transition temperature (amorphous plastics) or the crystallization temperature (semi-crystalline plastics) is beneficial for replication.

Introduction of an interfacial thermal resistance at the cavity surface will slow the solidification of the melt, and has been shown to improve replication (*17, 18, 31*). A similar effect is achieved with an insert made in a material with a lower thermal diffusivity, e.g. using a non-metallic material (*32, 33*).

2.3. Injection speed

Raising injection speed increases pressures within the cavity during filling, and also raises melt temperature due to viscous heating. Higher injection speed has generally been found to improve replication (*15,18,19,22, 27, 31*).

2.4. Micro-feature location, distance from gate

Features close the gate experience higher pressures during filling, before the compression and holding pressures come on. However, they also experience a longer cooling time during filling; thus opposing influences exist. Feature replication along the flow direction can therefore vary due to a different balance between these (*13, 18, 31, 34*).

2.5. Feature orientation relative to melt flow

Linear molded features, such as channels or raised ridges, may show different results depending on their alignment relative to the melt flow direction. It is generally found that

features parallel to flow are better replicated than those transverse to the flow. A factor may be that air is trapped in or against transverse features, whereas it is more easily displaced ahead of the melt in parallel-to-flow features. Also, the deformation required for the plastic to replicate transverse features may be larger, for example on the downstream side of raised ridges on the master (*11, 13, 19, 31*).

2.6. Holding pressure and duration

As expected, it is widely found that higher holding pressure improves replication (*7, 11, 15, 16, 18, 22, 23, 35, 36*). Where this is not so, the reason may be the pre-existence of a thick frozen layer resisting deformation. Alternatively, over-packing may make de-molding more difficult, resulting in micro-feature damage (*37*).

2.7. Cavity evacuation

Trapping of air in a recessed molded feature, or against a raised one can prevent complete replication. Because of the rapidity of the process, compression will be effectively adiabatic, and can result in high pressures that resist melt flow, together with temperatures sufficiently high to burn the plastic. Failure to vent cavity air at the parting surfaces of the mold will exacerbate the problem, but it may also be necessary to evacuate the cavity before melt injection. Reports of improved replication following cavity evacuation include (*38, 39*).

2.8. Plastic properties

The relevance of the glass transition or crystallization temperature has been mentioned in relation to the melt fluidity under given process conditions. However, materials with the same glass transition temperature can have different viscosities at the same temperature. Comparing two PMMAs with the same glass transition temperature, but different molecular weights, it was shown how the one with the lower molecular weight and lower viscosity provided better replication (*24*). COC is often found to give good replication on account of its

low viscosity and low shrinkage, and has been ranked (in order) above PS, PC and PMMA (*22*). The flexibility of thermoplastic elastomers can assist replication by avoiding de-molding damage (*27, 40*).

2.9. Raised versus recessed molded features

Molding raised features, such as ridges, pillars or micro-needles, requires plastic to fill recesses, such as grooves or holes, in the master. Solidification rate within these will be governed by a Fourier number for heat conduction containing the square of a length scale corresponding to the recess dimensions, for example the diameter of a hole. For small dimensions, the Fourier number becomes large at short times, corresponding to very rapid solidification, limiting achievable feature aspect ratios and leading to poor replication (*41*). Molding recessed features, such as channels, requires plastic to envelop raised features, such as ridges, on the master. Here the length scale is the thermal penetration depth representing a cooled layer thickness, and replication may be possible on longer time scales.

2.10. Molding micro-fluidic channels

In reference (*42*) micro-fluidic channels 20 – 200 μm wide by 100 μm deep were molded in PC and COC. Melt injection temperatures were set to the manufacturer's recommended maximum, and mold temperature was varied from 30°C to 120°C. Injection speed was varied from 10 – 70 cm/s. The radius of rounded upper channel corners was examined. For PC this reduced from 70 μm at the lowest mold temperature and injection rate, to close to zero at the highest values, the effect of tool temperature being most marked at low injection rates. For COC the corresponding figures were 110 μm reducing to zero. Glass transition temperatures of the materials were not quoted, and the influence of holding pressure and duration was not examined.

Reference (*43*) used an insert with ridges 2.6μm high, with top and base widths about 2 and 3 μm, spaced at about 3 μm. The insert surface was heated by infrared before melt injection,

and replication was assessed in terms of the depth of the molded channels. Using PMMA, full depth was obtained with a pre-heat temperature of 110°C, which was described as above the glass transition temperature. Increasing the holding pressure from 40 to 70 bar allowed complete replication at the lower temperature of 99°C, but further reduction below the glass transition temperature negated the effect of increased pressure. Reduced depth of the molded channels here no doubt results from incomplete melt flow into the spaces between the closely spaced ridges on the insert. The influence of other process parameters was not examined.

Reference (*22*) examined the influence of melt and mold temperature, injection velocity and holding pressure using an insert with ridges 30μm high by 100 μm wide with an 8° draft, spaced at 50 μm. The upper channel width was measured, including the rounded corners, on moldings in COC, PC, PS and PMMA. Improvements were seen for higher values of all parameters, with mold and melt temperature having most influence. Best results were obtained with COC, ascribed to its low viscosity and isotropic shrinkage. Reference (*25*) used a similar mold, pre-heated by passing a high velocity 500°C gas jet through it. In moldings in a PC with glass transition temperature 144°C complete replication was achieved with a pre-heat temperature of 150°C.

Reference (*12*) used an insert with ridges 75, 48 and 20 μm wide by 110μm high. Melt and mold temperature and injection speed were varied at two levels, within the usual processing range. Moldings in polypropylene achieved complete replication at all process conditions, no doubt due to the low viscosity of the polymer melt. Further works, where elevated tool temperature appears to have been used, but without comparison of different levels, include (*44-47*).

2.11. Review conclusions

The foregoing review makes clear the influence trends of processing parameters and the general requirements for successful replication of micro-features. However, interactions

between parameters have not been well explored. Fluidity or, more generally, the deformability of the plastic is essential, and this is promoted most strongly by a raised cavity surface temperature; hence the widespread use of variothermal injection molding, where the cavity surface is pre-heated before melt injection. But a further requirement is the simultaneous application of a sufficient melt pressure. The absence in the reviewed works of continuous in-cavity melt pressure measurements, together with simultaneous insert surface temperatures, makes it impossible to assess the extent to which this is achieved. Relevant here are the details of the cooling stage which follows melt injection. In many cases no information is provided on this; for example, how soon after cavity filling the cooling is started in a variothermal temperature cycle process. If too soon, the beneficial action of melt pressure during compression and holding may be lost. However, once replication is achieved, it must be locked in by rapid solidification before the holding pressure reduces. The present work aims to confirm these ideas and provide further insights.

3. Experimental

3.1. Trial molding and mold insert

The trial micro-features to be molded are derived from micro-fluidic circuits used for the micro-encapsulation of medical reagents. They include a T-junction of 70μm channels (circuit *a*) and a cross-junction of 100μm channels (circuit *b*), both fed by 400μm channels, all of square cross section. An insert with raised ridges to produce the molding was micro-milled in brass and is shown in plan in Figure 2. This also carries a further circuit with typical micro-fluidic features, which were not examined in the present work. The insert is set centrally into an experimental multi-functional tool that produces a rectangular plaque 165 x 100 x 3 mm.

3.2. Multi-functional mold

The cavity of the multi-functional mold is formed between copper alloy plates (Ampco®, Ampcoloy 940) separated by an interchangeable stainless steel spacer frame allowing molding of plaques of different thicknesses. In the present work this was 3mm thick. The plates are each drilled with eight 8 mm diameter holes for coolant water flow perpendicular to the melt injection direction. Twelve cartridge heaters (Watlow, Firerod®) are set into the back of each half of the mold, providing 3 kW heating on each side. Melt supply to the cavity is via a coat hanger-type distribution channel followed by a flow restriction, designed to produce a flat flow front. Ejectors are positioned outside the area of the insert.

3.3. Instrumentation

The mold and cavity are provided with comprehensive instrumentation. Figure 3 shows the locations of thirteen thermocouples (TC) in the fixed and moving cavity plates. These are 1mm diameter, steel sheathed, mineral insulated K-type thermocouples, and are located in holes drilled from the back of the copper plates with their tips 2mm below the cavity surface. The tip of TC11 is similarly located centrally in the insert. Pressure sensors are located just after the gate, at a central position and near the end of the flow path. These 2.5mm diameter piezo-electric sensors (Kistler Type 6158A) are flush mounted with the cavity surface. TC11 and pressure sensor 2 are used to provide conditions relevant for the micro-feature moldings, while the other TCs provide information on temperature uniformity over the plates. Values are logged at a frequency of 10 Hz using a data acquisition and control system (DAQ, National Instruments Corporation).

3.4. Mold heating and cooling, and data logging and control system

To implement variothermal injection molding, electrical resistance heating is alternated with water cooling. At a local level the cartridge heaters are controlled by a self-tuning three term

controller (West Instrument) with the facility to switch between two set points using an externally generated signal. TC4 is the control thermocouple. The upper set point is related to the desired cavity temperature, and switching to this initiates heating. Switching to the lower set point shuts off heating. Cooling is provided by a chiller operating at 12°C. Tool inlet and outlet water temperatures are logged. A compressed air blast is used between cooling and heating to clear water from the tool.

The heating-cooling cycle is controlled at the supervisory level by the DAQ system programmed in National Instruments LabVIEW in Windows. User inputs include temperature set points, a hot dwell time after the tool reaches the set temperature, a cold temperature (end of cooling), a cool dwell time before the air blast, air blast duration, and the duration of pressure monitoring. Generated digital outputs include set point switching on the temperature controller, start and stop pressure measurement, allow injection, mold open, and start and stop air blast. Full details of the experimental equipment and procedure are available in reference (*48*).

3.5. Microscopy of the insert and moldings: qualitative assessment of replication

Figure 4 is a scanning electron microscope (SEM) image of the micro-milled insert. This shows circular milling marks and a distinctive band of parallel milling marks at the foot of the ridge. Transcription of these onto the molding provides useful insights into the replication process. As explained in the Section 1 Introduction, micro-feature replication is assessed by measuring the outer width at the top of the molded channels and comparing it with the width at the base of the mold insert. In poor replication the outer width on the molding is increased because plastic has not filled the base corner of the ridge on the tool insert, leaving a rounded upper corner on the channel. This is seen in the digital microscope images Figure 5 and Figure 6, which compare poor and better replication. The rounded corner

has a smooth surface and shows a clear boundary with the region that has contacted the insert surface, where milling marks, as visible in Figure 4, are reproduced. Note particularly the marks adjacent and parallel to the base of the ridge wall. It is clear that these are not reproduced on the molding shown in Figure 5; instead, we see a smooth region which is the rounded upper corner of the molded micro channel. In Figure 6, the marks at the foot of the ridge are more completely transcribed, and the smooth region is narrower, indicating that plastic has made more complete contact here.

3.6. Quantitative assessment of replication

Chosen positions for examination and measurement of the moldings and comparison with the insert are defined on Figure 2. These include locations on parallel-to-flow and transverse features of all three sizes. The relationships to features on the (unexamined) serpentine circuit are used to help define these positions.

Outer channel widths on the moldings, see Figure 1, have been measured using a digital microscope (Keyence VHX-1000E with Keyence VH-Z100UW lens). A rigorous assessment of measurement uncertainties was carried out. Confidence limits resulting from random errors were established using Student's t-test, and extended to account for uncertainties arising from possible systematic errors. The digital microscope calibration was also repeatedly checked.

These dimensions are to be compared with the width at the base of the insert ridge. This proved impossible to measure with the digital microscope, as the out-of-focus side walls interfered with the definition. A white light interferometer (Veeco WYKO NT2000) was therefore used. Measurement confidence limits were again carefully established. Comparison of insert ridge top measurements at the same position by the two instruments showed no significant differences at the 99% confidence level, providing assurance on the comparability of the measurements.

3.7. Experimental molding program

Moldings were made in the medical grade PMMA, Altuglas SG7 (Arkema), a suitable material for micro-fluidics. This has glass transition temperature (Tg) 104°C (manufacturer's data). The variables in the molding program relate to the variothermal process, namely the temperature to which the insert surface is heated before melt injection and the time after filling at which cooling is started. Other process parameters were kept constant, using manufacturer's recommendations, as summarized below:

Barrel Temperatures: nozzle 226 °C, zone 4 232 °C, zone 3 226 °C, zone 2 226°C, zone 1 221 °C, feed 55 - 70 °C.

Velocity control (injection) phase: volumetric flow rate 60300 mm^3/s; filling time approx. 1.1 s.

Velocity-pressure switchover point: by screw position, at 18.5 mm for process conditions A and B, then 17.5 mm for all following processing conditions.

Pressure control (holding) phase: machine hydraulic pressure 55 bar, duration 10 s.

Machine intensification factor 6:1.

Rotational screw speed for charging phase: approx. 99 rpm.

The trial program is detailed in Table 2. It should be noted the manufacturer's recommended mold temperature is 66 °C.

Repeat moldings at each set of conditions were highly reproducible: peak cavity melt pressures agreed within 8 bar (3%) and dimensional measurements on the moldings to within the determined 99% confidence limits.

3.8. Simulation of plastic cooling and material property variations around the glass transition

As the results of the molding trials are presented below, they will be interpreted using information on the extent of plastic melt cooling together with the accompanying melt cavity pressures. To assess the melt cooling, numerical simulations are carried out. The transient one-dimensional heat conduction equation (x-direction, perpendicular to the cavity surface) is solved using the implicit first order backwards finite difference method. The time dependent boundary condition at the cavity surface is provided by the measured mold insert temperatures and the symmetry condition is applied at the cavity mid-plane. Constant physical properties are assumed and obtained from the literature, see Table 3. Interest focusses on early stages of cooling, including during filling. As the insert is located at the center of the cavity, it experiences melt flow for approximately 0.5s. During this short initial period, calculations (not detailed here) show that the convective (y-direction) heat transfer brought about by melt flow is small relative to the x-direction heat conduction, and is therefore neglected. This is justified on the basis of the very steep x-direction temperature gradients near the cavity surface during the initial moments of cooling and the low flow velocities close to the surface, which are further reduced as cooling and solidification proceed. In other words, local Graetz numbers very close to the cavity surface are low. The relevant cooling period extends to several seconds, of which the filling phase occupies only a small part.

It has been widely asserted that replication is hindered when the plastic temperature is low relative to Tg. However there has been no discussion in this context of material property variations close to Tg, and it is important to be aware of these in order to interpret the influence of various degrees of cooling upon replication. Reference (*49*) studied the behavior of a PMMA in uniaxial compression tests. At Tg a distinct yield point was found, followed

by a period of strain hardening, which can be expected to hinder deformation of the plastic and limit replication. As the temperature was raised, these phenomena faded and fluid-like behavior developed at about 20°C above Tg. It therefore appears that Tg +20 = 124 °C in the present case is a significant temperature in relation to replication. From the cooling simulations we accordingly calculate the thickness of a 'transitional' layer adjacent to the tool (insert) surface where the plastic temperature is below 124 °C.

4. Micro-channel replication results

4.1. 400μm channels parallel-to-flow

Figure 7 and Figure 8 plot the channel top widths versus the varied process conditions (insert temperature and cooling start time) for locations on the parallel-to-flow channels. Also shown is the target value corresponding to the ridge base width on the insert. All values are shown with 99% confidence limits determined as described above. Results for each process condition are discussed in turn and interpreted with the help of data on the calculated transitional layer thickness in combination with cavity pressures. The figures show significant differences (at the 99% confidence level) as the processing conditions are changed. They also show significant differences between locations for a given process condition. These are thought to be due to temperature variations over the insert. Examination of the thermocouple readings showed that variations along the long axis of the insert were small, but across the shorter dimension variations of a few degrees occurred, with temperatures higher near the center. Thus, by interpolation into the readings, a difference of 3.7 °C is estimated between locations a2 and a1 for process condition A, rising to 6.9 °C for process condition D. Between locations b3 and b1 differences of approximately 5.1 °C and 9.5 °C are estimated for A and D respectively. In most cases locations with the higher temperatures show better

replication. It is therefore more precise to interpret the specified process conditions in terms of a nominal insert temperature.

Process condition A: With the mold insert at 81°C replication at all positions is poor, with rounded upper corners of the channels increasing their outer widths to about 50μm greater than the target value. The plastic has been unable to flow completely into the corners at the base of the ridge on the mold insert; flow has ceased when the radius of curvature of the free surface is about 50 μm. This is also apparent from the failure of the molding to replicate the milling marks close to the base of the ridge. Compare Figure 4 with Figure 5.

Process conditions B, C: Raising the mold insert temperature to 98°C and then further to 109°C improves replication significantly, bringing values at several locations within the target range. Figure 6 shows how milling marks close to the ridge base are now more fully replicated for process condition C.

To provide insights into the replication process, plots showing the cavity melt pressure evolution, the insert surface temperature, and the development of the transitional layer thickness are used. The time datum is when the melt enters the cavity as detected by PS 1, see Figure 3. For proves condition A, see Figure 9, due to the low insert temperature (81°C), transitional layer formation is rapid. When peak cavity pressure is reached at the end of the compression phase, the transitional layer thickness is already 300 μm. Raising the insert temperature to 98 °C, process condition B see Figure 10, delays the transitional layer formation. When the pressure is approaching its maximum value, the layer thickness is around 200 μm. For process condition C (109°C), see Figure 11, the transitional layer thickness at peak pressure is 125 μm, while thicker layers form later in the holding phase where pressures are falling. This reduction in transitional layer thickness at peak pressure time correlates closely with the improvement in replication seen in Figure 7 and Figure 8, as insert temperature is raised, moving from condition A to C. The results show how good

replication is achieved if a high melt pressure exists while the transitional layer is sufficiently thin. Incidentally, note the slight increase in peak cavity pressure as the insert temperature is raised, due to better transmission of the holding pressure resulting from thinner transitional layers. It appears from Figure 10 that a layer thickness of around 300 μm is already too thick to be forced into good contact with the insert under the prevailing pressure of 300 bar. The quantitative aspects of these conclusions no doubt depend on the feature geometry and plastic material, and can form the subject of further research (we mention the effect of feature size below).

Process condition D: Raising the insert temperature further to 122 °C produces a mixed result. A significant reduction in replication quality is seen at locations b2, b3, b4 as compared with condition C. Changes at positions a2, a3 and b1 are non-significant, while a significant improvement is seen at a1. Examination of SEM images of positions b2, b3 and b4 shows that the parallel milling marks at the foot of the insert ridge are well replicated, indicating that plastic has made good contact there, see Figure 11. The width at the top of the molded channels is, however, outside the target range and about 7 μm greater than for condition C. Figures 12 and 13 compare the pressure profiles and transitional layer development for conditions C and D. We see how raising the insert temperature from 109 °C (C) to 122 °C (D) has delayed development of the transitional layer. For condition C it has reached a thickness of 350 μm when cooling is switched on at 12.4s, while for D it has reached only 150 μm. By the time it reaches 350 μm the melt pressure has fallen to about 110 bar, which is 200 bar below the peak pressure at the end of compression. It appears that for condition D at locations b2, b3 and b4 plastic has been forced into good contact with the insert during compression, but that falling holding pressure in the presence of only a thin transitional layer has allowed the plastic to retract from contact with the insert, resulting in increased upper channel widths. In contrast, for condition C, a thicker transitional layer has

been able to lock in the replication before the melt pressure has fallen significantly. Spring-back in hot embossing has been observed and constitutive modelling of material properties near Tg undertaken to characterize it in reference (*50*). There remains the question of why this phenomenon is seen only at locations b2, b3 and b4. We suggest this is related to temperature variations over the insert. As noted in Section 4.1 under condition D location b1 is about 10°C hotter than b3, and a1 about 7 °C above a2. Thus retraction is seen at the locations that are hotter and also further upstream, where the transitional layers will be thinner. These unexpected results were confirmed on a number of molded samples, and conflict with the prevalent idea that raising the mold temperature always improves replication; they show how the interaction with cooling and melt pressure must also be taken into account.

Process Condition E: Conditions are as for D, except that cooling switch-on time is brought forward from 12.3 to 3.4s. Faster transitional layer development, see Figure 14, appears to have prevented the retraction postulated for D and replication is now as in C or better. However, the insert temperature here is higher than in C (123°C as compared with 109°C) and earlier cooling allows taking full advantage of the resulting higher melt fluidity, without the deleterious effects of retraction. Replication is now complete.

Process conditions F, G: Cooling is brought further forward to 2.4 and 1.4s, see Figure 15. As this occurs we find deterioration of the replication at positions a1, and a2, and then also at b1, b2 and b3, see Figure 16. These locations all lie downstream of transverse features, and channel top width is found to increase, and replication of the milling marks to deteriorate, with increasing distance downstream of these. This unexpected and previously undescribed effect appears to be connected with early cooling and rapid transitional layer formation hindering melt flow downstream of the transverse ridges on the insert. Channel widths for

these positions are not plotted on Figure 7 and Figure 8. A full explanation of this effect would probably require detailed simulations of melt flow and heat transfer, which are beyond the scope of the present work.

Process conditions H, I, J: Cooling switch-on is further advanced to 0.4s (which is during filling, see Figure 17), and for I and J the insert temperature is raised to 131°C and then to 141°C. Replication at locations a3 and b4 remains unchanged, whilst deterioration downstream of transverse features continues.

4.2. 400µm channels transverse to flow

Results for positions a4 and b5 follow a pattern very similar to those discussed above for parallel-to-flow channels, namely a marked improvement from process conditions A to B to C. For D a small deterioration is seen at position b5, postulated as retraction, and no significant deterioration at a4, where the temperature is a few degrees lower. The result at b5 is improved by earlier cooling switch-on in F. A new phenomenon is seen as cooling is brought further forward. Under process conditions G, H and I replication on the downstream side of transverse features deteriorates; plastic is unable to flow fully into the downstream corner at the base of the insert ridge. This is visible in Figure 18, where it can be seen that the milling marks are less well replicated on the downstream side. An increase in tool pre-heat to 131°C in process condition I, and further to 141°C in J, heals this defect.

4.3. 100µm Channels

Positions b6 and b7 are on the 100µm channels forming the cross junction, see Figure 2, respectively on the parallel-to-flow and transverse arms. In general, good replication appears easier to achieve for these smaller channels, see Figure 19. Already for process condition B replication at the two positions is within or close to the target range, and remains within it for most of the other conditions. Notably, the deterioration previously noted at some positions in

process condition D is not seen. It appears that less stretching of the plastic is required to fill the base corner of the insert ridge because it is smaller, resulting in a reduced tendency to retraction. As cooling switch-on is brought forward in G (to 1.4s) and H (0.4s) a deterioration in replication of the transverse channel at location b7 is seen, as already noted for the 400μm channel, and for the same reason; namely that melt is less able to flow into the base corner on the downstream side of the inert ridge. Also, as before, further tool temperature increase (process conditions I, J) heals this defect.

4.4. 70μm Channels

Positions a6 and a5 are located on the 70μm channels forming the T-junction, respectively parallel to and transverse to flow. Previously described trends are consistently maintained, with replication generally becoming easier, falling within the target range by process condition C, see Figure 20. No deterioration is seen for D (no retraction). Significant deterioration occurs only with early cooling switch-on (in G and H) for the transverse position a5, but not for the parallel to flow a6, consistent with the previously noted deterioration of replication on the downstream side of transvers features. Higher tool temperature (I, J) cures this, bringing both positions back onto target.

5. Conclusions

A common defect in molding micro-channels arises from the failure of plastic to fill the corner at the base of the ridge on the tool insert, which results in the molded channels having rounded upper corners. As the advancing flow front passes over the ridge, melt pressure is initially low and insufficient to overcome viscous and elastic forces resisting flow into the corner, leaving an unfilled region, as illustrated in Figure 1. Surface tension of the melt is not a factor here. The ratio of melt pressure to the Laplace pressure jump across a (cylindrical) free surface with radius 50 μm can be shown to be of the order of 10^3, using surface tension

data for PMMA from reference (*51*). To complete filling, higher melt pressure is necessary, but this must be applied before a frozen layer is formed that is thick enough to resist deformation. In the present work the thickness of a transitional layer having solid-like properties has been calculated as a function of time by finite differences, using measured transient insert surface temperatures as a boundary condition. In contrast to previous work where it has been assumed (sometimes tacitly) that 'freezing' of the plastic – i.e. cooling below the glass transition temperature (Tg) – is a determinant for replication, we take account of studies that show that the properties of PMMA become fluid-like only at 20°C above Tg. We accordingly define a 'transitional' layer as that where the temperature is below Tg + 20 = 124°C. Additionally, melt pressures have been measured in the cavity, including at the location of the micro-features. Thus it has been possible to identify melt pressures at the time of formation of transitional layers of various thicknesses. In terms of these it has been possible to construct a consistent explanation of how and why micro-feature replication quality correlates with injection molding process conditions. Notably, this was not possible using the thickness of a 'frozen' layer with temperature below the glass transition temperature itself, confirming the significance of the chosen temperature 20°C above Tg at which the plastic exhibits fluid-like properties. For the 400μm channels it is very clear that improvements in replication - completion of the filling of the base corner of the insert ridge - correlate inversely with the thickness of the transitional layer when peak pressures are reached at the end of the compression phase of the molding cycle. The development of the transitional layer depends on the temperature of the insert surface as melt is injected (melt injection temperature is maintained constant here) as well as the timing of cooling switch-on. Under process condition A (insert at 81°C, cooling on at 12.3 s) a 300μm layer (comparable to the feature size) has formed by the end of compression, and this is sufficient to resist deformation, resulting in poor replication. Raising the insert temperature to 98°C and 109°C

(B, C) slows development of the transitional layer, which reaches 200µm and 125µm respectively at the end of compression. A corresponding improvement in replication is seen. Further increase in the tool temperature to 122°C (D) see Figure 13, result in slow layer development until cooling is switched on at 12.4 s, when pressure has already fallen significantly below its peak value. For this case an interesting phenomenon was observed. At three locations a significant deterioration in replication is seen. The molding replicates the distinctive milling marks in the base corner of the insert ridge, indicating that the plastic has made full contact; however, the channel top widths are up to 10µm oversize. It appears that the plastic has retracted as melt pressure falls from its peak while the transitional layer thickness is only 150µm. Apparently, this layer thickness is insufficient to lock in the replication. In contrast, under process condition C a layer of 350µm was able to achieve this. It is interesting to note that a layer of similar thickness, coinciding with peak pressure at the end of compression was sufficient to prevent good replication in PC A. The results from process condition D show that raising the tool temperature does not always lead to an improvement in replication. To benefit from the improved melt fluidity at higher temperatures, it is essential to freeze in the deformation while the melt pressure is close to its peak value. This can be achieved by bringing forward the cooling switch-on time. Increased tool temperature and earlier cooling have opposing effects in determining transitional layer formation, and, by balancing these, formation of a layer thick enough to lock in replication can be timed to occur before melt pressure falls excessively. This is broadly what is achieved in process conditions F – J, where tool temperature is raised in steps to 141°C, and cooling switch-on is brought forward successively to 3.4, 1.4 and 0.4s. However, caution is needed in using early cooling. We find that deterioration in replication occurs in parallel-to-flow features lying downstream of transverse features. In the presence of early cooling, transverse 400 µm ridges appear to disrupt melt flow and interfere with frozen layer formation. The

details of this remain unclear. A further deleterious effect of early cooling is seen in replication of the transverse features themselves. Flow into the base corner of the insert ridge on the downstream side is less good (G, H); however, raising the insert temperature further (I 131°C, J 141°C) cures this defect.

Considering now the smaller (100µm and 70µm) features, it is found that replication is generally easier and less susceptible to the types of defect described above. The initial defects in the channel top widths, for process condition A, are around 35µm for the smaller features, compared with about 50µm for the 400µm channels. The smaller raised ridges on the insert perturb the flow less, and less deformation of the plastic is required to fill the base corner. Thus, as the features become smaller, lower tool temperatures and melt pressures are required for replication. The retraction effect found at some positions for process condition D disappears. Less good replication on transverse features is, however, still evident for both 70µm and 100µm channels due to difficulty in filling the base corner of the insert ridge on the downstream side, but this is resolved at the highest insert temperatures. No deterioration downstream of a transverse feature is observed with early cooling at position b1, no doubt because this 70 µm ridge perturbs flow less than the 400µm ridge.

This general behavior is in marked contrast to what is found when attempting to mold raised features, such as pins or pillars, as already discussed. In molding recessed features, it appears that, within the range presently studied, smaller features are more readily replicated.

In the present work a particularly detailed examination and discussion of micro-feature replication in injection molding has been possible. Features have been examined at several positions on the molding, showing the influence of their location, orientation and size. In contrast to previous works, the simultaneous availability of cavity melt pressure and the thickness of a cooled transitional layer with solid-like properties shows how these interact to

determine the replication achieved. In a variothermal molding process, the temperature to which the mold insert is heated before melt injection and the cooling switch-on time combine to control the transitional layer thickness development, and provide the means to achieve the correct relationship of this with melt pressure to provide satisfactory feature replication. Where this is not achieved, a number of phenomena that can adversely affect replication have been identified. The present work provides insights and guidance on setting process conditions in variothermal injection molding to achieve mass production of accurately replicated micro-fluidic circuits and more generally of any product with recessed functional micro-features.

Acknowledgements

This work was funded by the Welsh Assembly Government UK/European Regional Development Fund (ERDF) under the Academic Expertise for Business Program as Collaborative Industrial Research Project HE 09 ROI 0810. Further work was carried out within the ASTUTE2020 project also funded through ERDF.

Access to resources at the Manufacturing Engineering Centre, Cardiff University, for manufacture of the mold insert, under the EUMinifab project, is acknowledged.

The authors are grateful to Dr Nick Croft, College of Engineering, Swansea University, for coding and running the finite difference calculations, and to Dr Daniel Palmer of Q Chip Ltd for assistance with micro-fluidics.

References

1. E. K. Sackmann, A. L. Fulton, D. J. Beebe, *Nature,* **507**, 181 (2014).
2. H. Becker, C. Gartner, *Anal. Bioanal. Chem.,* **390**, 89 (January, 2008).
3. H. N. Hansen, R. J. Hocken, G. Tosello, *CIRP Annals - Manuf. Technol.,* **60**, 695 (2011).

4. M. Gad-el-Hak, Ed., *The MEMS Handbook: Design and Fabrication*, (CRC Press, Taylor and Francis Group, Boca Raton, London, New York, 2nd Ed., (2006).

5. P. Abgrall, A. M. Gue, *J. Micromech. Microeng.,* **17**, R15 (2007).

6. G. Bissacco, H. N. Hansen, P. T. Tang, J. Fugl, in *American Society of Precision Engineers Conference*, Spring (2005).

7. G. R. Berger, D. P. Gruber, W. Friesenbichler, C. Teichert, M. Burgsteiner, *Intl. Poly. Proc.,* **26**, 313 (2011).

8. M. Yoshii, H. Kuramoto, Y. Ochiai, *Polym. Eng. Sci.,* **38**, 1587 (1998).

9. G. Lucchetta, M. Fiorotto, P. F. Bariani, *CIRP Annals - Manuf. Technol.,* **61**, 539 (2012).

10. K. J. Cha, M.-H. Na, H. W. Kim, D. S. Kim, *J. Micromech. Microeng.,* **24**, (2014).

11. N. Zhang, J. S. Chu, C. J. Byrne, D. J. Browne, M. D. Gilchrist, *J. Micromech. Microeng.,* **22**, (June, 2012).

12. G. Tosello, F. Marinello, H. N. Hansen, *Plastics, Rubber and Composites,* **41**, 29 (2012).

13. C. H. Yang, H.-X. Huang, J. M. Castro, A. Y. Yi, *Polym. Eng. Sci.*, 959 (2011).

14. M. S. Huang, H. H. Ku, *J. Appl. Polym. Sci.,* **122**, 3446 (2011).

15. G. Fu, S. B. Tor, D. E. Hardt, N. H. Loh, *Microsyst. Technol.,* **17**, 1791 (2011).

16. M. S. Huang, J. C. Yu, Y. Z. Lin, *J. Appl. Polym. Sci.,* **118**, 3058 (2010).

17. T. C. Hobaek, M. Matschuk, J. Kafka, H. J. Pranov, N. B. Larsen, *J. of Micromech. and Micro Eng.,* **25**, (2015).

18. G. Lucchetta, M. Sorgato, S. Carmignato, E. Savio, *CIRP Ann-Manuf Technol.,* **63**, 521 (2014).

19. P. Hernandez, A. Murawko, J. Martinez, G. Pelaez, E. Ares, *Procedia Eng.,* **63**, 885 (2013).

20. H.-Y. Lin, C.-H. Chang, W.-B. Young, *Int. Communications in Heat and Mass Transfer,* **37**, 1477 (2010).

21. S. H. Kim, J. H. Jeong, J. R. Youn, *Nanotechnol.,* **21**, (2010).

22. C. S. Chen, S. C. Chen, W. H. Liao, R. D. Chien, S. H. Lin, *Int. Communications in Heat and Mass Transfer,* **37**, 1290 (2010).

23. G. R. Berger, D. P. Gruber, W. Friesenbichler, C. Teichert, M. Burgsteiner, *Int. Poly. Proc.,* **26**, 313-322 (2010)

24. S. Kuhn, A. Burr, M. Kubler, M. Deckert, C. Bleesen, *J. Micromech. Microeng.,* **21**, 17 (2011).

25. S. C. Chen, J. A. Chang, W. Y. Hsu, S. W. Huang, *Microelectron. Eng.,* **88**, 1594 (2011).

26. K. Bobzin *et al.*, *Production Engineering Research and Development,* **5**, 415 (2011).

27. S. H. Yoon *et al.*, *Polym. Eng. Sci.,* **50**, 411 (Feb, 2010).

28. K. Park, S.-I. Lee, *J. Micromech. Microeng.,* **20**, (2010).

29. Y. E. Yoo *et al.*, *Curr. Appl .Phys.,* **9**, e12 (2009).

30. H. S. Carslaw, J. C. Jaeger, *Conduction of Heat in Solids*, (Clarendon Press, Oxford, 2nd Ed. (1959).

31. J. G. Lee, B.-K. Lee, T. G. Kang, T. H. Kwon, *Poly. Eng. & Sci.,* **50**, 1186 (2010).

32. R. H. Pedersen, Q. Xu, J. M. Stormonth-Darling, N. Gadegaard, *Macromol. Mater. Eng.* **300**, 172 (2015).

33. R. K. Jena, C. Y. Yue, K. X. Yun, *RSC Adv.* **4**, 12448 (2014).

34. Y. E. Yoo *et al.*, *Trans. Nonferrous Met. Soc. China* **21**, S148 (2011).

35. K. L. Yung *et al.*, *J. Micromech. Microeng.* **22**, (2012).

36. S. H. Park, W. I. Lee, S. N. Moon, Y.-E. Yoo, Y. H. Cho, *eXpress Polymer Letters* **5**, 950 (2011).

37. M. Matschuk, H. Bruus, N. B. Larsen, *Microelectron. Eng.* **87**, 1379 (2010).

38. V. Kalima *et al.*, *Opt. Mater.* **30**, 285 (2007).

39. Z. Lu, *International Journal of Advanced Manufacturing Technology* **40**, 490 (2009).

40. S. Birkar, J. Mead, C. Barry, *Rubber Chem Technol* **87**, 629 (2014).

41. G. J. Xu, L. Y. Yu, L. J. Lee, K. W. Koelling, *Polym. Eng. Sci.* **45**, 866 (2005).

42. R. K. Trichur, MSc Thesis, Dept. Electrical and Computer Engineering and Computer Science, University of Cincinnati, USA (2003).

43. M. C. Yu, W. B. Young, P. M. Hsu, *Mater. Sci. Eng. A-Struct. Mater. Prop. Microstruct. Process.* **460**, 288 (2007).

44. O. Larsson *et al.*, in *Int. Conf. on Solid-state Sensors and Actuators*. (Chicago, USA), **2**, 1415-1418 (1997).

45. D. S. Kim, S. H. Lee, C. H. Ahn, J. Y. Lee, T. H. Kwon, *Lab. Chip* **6**, 794 (2006).

46. K. O. Andresen *et al.*, *J. Micromech. Microeng.* **20**, 9 (2010).

47. D. A. Mair, E. Geiger, A. P. Pisano, J. M. J. Frechet, F. Svec, *Lab. Chip* **6**, 1346 (2006).

48. P. G. Wlodarski, PhD Thesis, College of Engineering, Swansea University, UK (2013).

49. A. Ghatak, R. B. Dupaix, *Int. J. of Structural Changes in Solids - Mechanics and Applications* **2**, 53 (2010).

50. D. Mathiesen, R. Dupaix, in *Annual Conference on Experimental and Applied Mechanics*, Lombard, IL, USA, 3 - 5 June (2013).

51. S. Wu, *J. Phys. Chem.*, 74 (3), 632 - 638 (1970).